Micro-Arcjet: Microfabrication with UV Lasers and Thrust Characteristics

IEPC-2005-123

Presented at the 29th International Electric Propulsion Conference, Princeton University, October 31 – November 4, 2005

Hideyuki Horisawa* and Tsuyoshi Noda†
Tokai University, Hiratsuka-shi, Kanagawa, 259-1292, Japan

Kosuke Onodera‡
Tokai University, Hiratsuka-shi, Kanagawa, 259-1292, Japan

and

Itsuro Kimura§
Professor Emeritus, University of Tokyo, Bunkyo-ku, Tokyo, 113-8856, Japan

Abstract: Preliminary DSMC simulations on internal and exhaust nozzle-flow characteristics of micro-arcjet nozzles including multi-mozzle arrays were conducted. It was shown that the use of the multi-nozzle array was effective in suppressing expansion of each under-expanding jet, and in inducing axially confined jets, through the interactions of the jet boundaries, or multi-jet effects. Microfabrication of micro-arcjet nozzles with fifth-harmonic Nd:YAG pulses (wavelength 213 nm) and their operational tests were also conducted. Micro-arcjet nozzles were machined in a 1.2 mm thick quartz plate. Sizes of the nozzle exit were 0.44 mm in height and constrictor height of 0.1 mm. For an anode, a thin film of Au (~ 100 nm thick) was coated by DC discharge PVD in vacuum on divergent part of the nozzle. As for a cathode, an Au film was also coated on inner wall surface. In operational tests, a stable discharge was observed for mass flow of 0.4 mg/sec, input power of 6 W. In this case, plenum pressure of the discharge chamber was 50 kPa. With 6 W input power, thrust obtained was 1.2 mN giving specific impulse of 147 sec with thrust efficiency of 7 %.

I. Introduction

The progress of micromachining techniques such as micro-mechanical machining systems and microelectromechanical systems (MEMS) has brought space engineering fields another good chance to challenge new innovative dreams.[1] One of the examples is that these techniques have enabled fabrication of various elements and parts of high-functional microspacecraft systems. Currently it has become possible for a combined fleet of the microspacecrafts orbiting the earth to perform critical and highly complex tasks with various high-functional electronic- and mechanical- devices. Capable microspacecrafts with distributed functionality are

* Associate Professor, Department of Aeronautics and Astronautics, email: horisawa@tokai.ac.jp.
† Graduate Student, Department of Aeronautics and Astronautics.
‡ Graduate Student, Department of Aeronautics and Astronautics.
§ Professor Emeritus, University of Tokyo.

envisioned to take over the tasks of more massive and expensive platforms with increased survivability and flexibility.

It is becoming increasingly evident that these microspacecrafts will require efficient propulsion systems to enable many of the missions currently being investigated.[1–4] Although in the past, many very small spacecraft have lacked propulsion systems altogether, future microspacecrafts will require significant propulsion capability in order to provide a high degree of maneuverability and capability. The system constraints on mass, power, maximum voltage, and volume with which microspacecrafts will undoubtedly have to contend will pose several challenges to overcome. Micropropulsion concepts that address these limitations in unique and beneficial ways will be of interest to the microspacecraft community.

The definition of micropropulsion is any propulsion system that is applicable to a microspacecraft which weighs less than 100 kg. This definition allows the inclusion of a wide range of concepts from scaled-down versions of existing thrusters operating at reduced power levels to completely redesigned thrusters using micromachining techniques. The mission requirements for microspacecraft will also be varied and, in some cases, a large range of capability might be required on the same spacecraft. Micropropulsion must be extremely versatile to address these requirements. It is clear that there is a need for these systems, which can be from high thrust chemical engines to high specific impulse electric thrusters, to fulfill specific missions, just as there is a need for larger spacecraft.[1]

The benefit of using electric propulsion for the reduction of spacecraft mass will likely be even more significant for mass limited microspacecraft missions. Feasibility studies of microspacecrafts are currently under development for the mass less than 100 kg with an available power level for propulsion of less than 100 watts. Various potential propulsion systems for microspacecraft applications, such as ion thrusters, field emission thrusters, PPT, vaporizing liquid thrusters, resistojets, microwave arcjets, pulsed arcjets, etc., have been proposed and are under significant development for primary and attitude control applications.[1]

Because of its system simplicity the arcjet thruster must be appropriate for the small-sized spacecrafts. Many of thrusters of this type with input power level of kilo-watts have been practically used in orbit such as north-south stationkeeping (NSSK) on geosynchronous satellites, etc. It has been reported in previous studies that a thermal loss to electrodes and a frozen flow loss are the primary loss mechanisms of the arcjet thrusters.[5–7] It has been confirmed that the thermal loss can be reduced at high-voltage mode discharge operation cases. Also, the frozen flow loss can be reduced at lower specific power input, or lower plasma temperature, operation, although a specific impulse will be decreased to some extent. In addition, it has been reported that an endurance of the arcjet is primarily determined by a degree of cathode erosion. From these facts, a significant suppression of those losses and cathode erosion can be expected with the use of the very low-power operation of the arcjet.

However, there has been little focus on the study of DC arcjets operational at very low-power levels, i.e., less than 100 watts, for microspacecraft propulsion devices, relating not only to the thrust performance but to fundamentals of the very low power DC discharges as well. Under these circumstances, authors have been investigating on both discharging and thrust characteristics of the very low-power DC arcjets.[8–16] Since the system can be simple and light-weight, possibly giving relatively higher thrust density and specific impulse, the very low-power arcjet must be appropriate for microthrusters unless its discharge is unstable under very low-power operation. In addition, very low-power operation of arcjets, especially at reduced specific power levels with lower temperature of the propellant which is heated through the discharge, will elongate the life of electrodes and reduce the electrode loss and frozen flow loss, resulting in higher thrust efficiency. Although the specific impulse achievable during operation will be reduced at low specific power levels, it will be recovered to some extent through the achievement of loss reduction.

The objective of this study is to investigate fundamentals of discharge characteristics and thrust characteristics of very low-power DC arcjets with electrical input power levels ranging from approximately 1 ~ 10 watts in order to ascertain an optimum operational condition which possibly results in higher thrust performance. In this study, investigations on conditions which give a stable operation were conducted, including evaluation of plasma characteristics through spectroscopic diagnostics of plasma in a discharge chamber. Also, thrust performances, such as thrust, specific impulse and thrust efficiency of the very low-power arcjet, was evaluated. Moreover, a preliminary study on microfabrication of micro-arcjet nozzles with fifth-harmonic Nd:YAG pulses was conducted. Investigations of conditions for a stable operation at input power of less than 10 watts and evaluation of thrust performances were carried out with the newly developed thruster.

II. Numerical Simulation of Micro-Nozzle-Flow for Optimum Configurations

A. DSMC Simulation of Internal Flows Micro-Nozzle Flow

The flow-through low-Reynolds number nozzle has been studied by several authors both experimentally and computationally.[20] In these studies, it was found that thick viscous boundary layers develop at Reynolds numbers below 1000, indicating poor nozzle efficiencies. The inefficiencies arise from the adverse interaction of the subsonic boundary layer with the core of supersonic flow causing the flow not to expand fully in the divergent nozzle section. In some cases, the viscous layer can occupy most of the divergent nozzle section.

From our recent experiments of thrust performance tests on micro-nozzles, it has been clear that the thrust performance of the very low-power micro-arcjet strongly depends on nozzle geometry. In designing an optimum micro-nozzle configuration, it is significantly important to consider the factors such as area ratio, pressure ratio, micromachining accuracies (geometrical accuracy, surface flatness, surface roughness), boundary layer thickness of inner nozzle wall, etc.

As for a preliminary simulation, assuming two-dimensional rectangular nozzles, internal flows in the micro-arcjet in operation were analyzed using a commercial computational fluid dynamics (CFD) simulation code (CFD2000, Adaptive Research, Inc.) employing the time-dependent compressive Navier-Stokes equation, in which typical conditions of the internal plasma obtained from operational tests were employed, i.e., plenum pressure of 80 kPa, total temperature of 1,500 K, mass flow rate of 1 mg/sec.

Figure 1 shows Mach number contours of internal flows of micro-nozzles with different area ratios, or exit heights of (a) 400μm and (b) 800μm with same constrictor heights of 100 μm. The viscous nature of the flowfield is apparent from the large subsonic boundary layer, and the core flow region with the maximum Mach number is restricted to a small portion of the flow near the centerline. Although maximum Mach numbers of both cases in the centerline regions are about the same, $M = 6$, the core flow region is much more restricted in a smaller divergent angle case ((a) 400μm-nozzle). While in a wider angle case ((b) 800μm-nozzle), relatively larger portion of the high Mach number region can be obtained.

Traditional continuum-based computational techniques employing the Navier-Stokes equation for the simulation of micro-nozzle flows can often provide erroneous or misleading results. These inaccuracies generally result during the computation of molecular transport effects. The macroscopic properties of any fluid flow may be identified with average values of the appropriate molecular quantities at any location within the flow. When this condition is not satisfied, there is a limit imposed on the range of validity of these continuum equations. This limit occurs when gradients of the macroscopic variables become so steep that the scale length is of the same order as the mean free path of the gas, or Knudsen number being greater than 0.01.

Because the flows through very small throat diameters even at large stagnation pressures result in relatively small Reynolds numbers, the predicted performance results obtained from Navier-Stokes solutions may be inaccurate. In the micro-nozzle flow predictions, it has been indicated that the Direct Simulation Monte Carlo (DSMC) method gives more accurate results for macroscopic performance characteristics.[20] The DSMC method provides means to simulate the flow of a general rarefied gas at the molecular level.

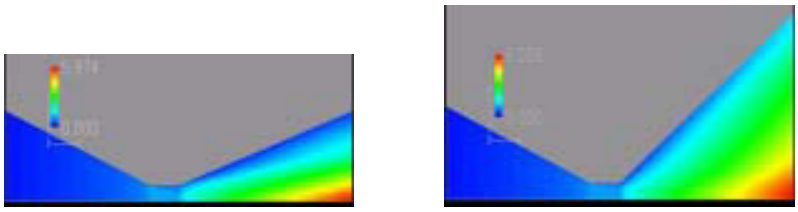

(a) 400 μm-nozzle. **(b) 800 μm-nozzle.**

Figure 1. Mach number contours of internal flows of micro-nozzles with different area ratios, or exit heights of (a) 400μm and (b) 800μm with same constrictor heights of 100 μm obtained with CFD simulation employing the Navier-Stokes equation.

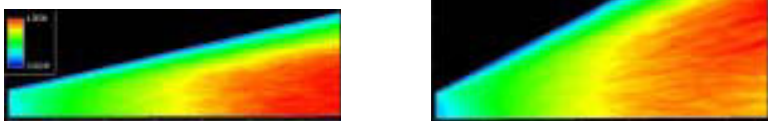

(a) 400 μm-nozzle. **(b) 800 μm-nozzle.**

Figure 2. Typical results of Mach number contours of internal nozzle flows obtained from DSMC simulation for the exit height of (a) 400 μm and (b) 800 μm with same constrictor heights of 100 μm (however with different length of divergent section from cases of Fig.1).

In order to investigate the optimum geometry, DSMC (Direct Simulation Monte Carlo) simulations for several micro-nozzle configurations were additionally conducted. Typical results of Mach number contours of internal nozzle flows are shown in Fig.2 for the exit height of (a) 400 μm and (b) 800 μm with same constrictor heights of 100 μm (however with different length of divergent section from cases of Fig.1). It can be seen that high Mach number regions of both cases in the centerline region is much more restricted in the smaller divergent angle case than the wider angle case. From these results for various micro-nozzle geometries, it was confirmed that the boundary layer thickness became lager especially in the narrow divergent angle nozzles indicating poor nozzle efficiencies than the wider angle nozzles.

B. DSMC Simulation of Micro-Nozzle Array

In this subsection, an investigation on advantages of use of the micro-nozzle array was conducted using a DSMC simulation code. Since our primary concern in this simulation was on the influences of interactions between under-expanded exhaust jet boundaries, a sonic condition was employed to each exhaust jet without calculating internal nozzle flows for simplicity.

Typical results of pressure distributions for two-dimensional quintuple nozzle cases for different nozzle-separations, i.e., (a) 100 μm, (b) 50 μm, (c) 25 μm, and (d) 0 μm are shown in Fig.3, in which each exit height of each nozzle element is 400 μm. As shown in these figures, pressure drops between the nozzles, or at separating points, at the exit tend to become less significant as the nozzle-separation decreases. Moreover in the smaller separation case, a higher pressure region tends to extend further in axial direction and also in normal direction perpendicular to a nozzle axis. It can be seen that the tendency of the extension of the high pressure region is more exaggerated especially in the center nozzle element.

Results of temperature distributions for the quintuple nozzle cases of Figs.3 (a) to (d) are shown in Fig.4. It can be seen in these figures that temperatures at separating regions between nozzles are getting higher as the nozzle-separation is increased. This is probably due to the increased rate of undirected or random motion of gaseous particles, and namely being thermalized. Meanwhile temperatures of the each center nozzle region are getting lower in smaller nozzle separation cases (although standard colors of each legend are different). This means that particles in these regions are less thirmalized and motions of the particles are more directed.

Results of distributions of Mach number, normal component and axial component of velocity vectors for the quintuple nozzle cases of Figs.3 (a) to (d) are shown in Figs.5 to 7, respectively. As can be seen in these figures, the normal velocity components, perpendicular to a nozzle axis, expanding between the nozzles, or to separating regions, at the exit tend to become significantly small as the nozzle-separation decreases. Namely, it is confirmed that the expansion of each expanding nozzle jet tends to become suppressed and axial velocity components and Mach number being augmented through the interactions of the jet boundaries.

Therefore, from these results, it is shown that the use of the multi-nozzle array is effective in suppressing expansion of each under-expanding jet, and in inducing more axially confined jets, through the interactions of the jet boundaries and the increase of the background pressure between the nozzles. Moreover, it is also expected that this effect of the increase of the static pressure at the nozzle exit will be transferred to an internal core flow in divergent nozzle section through a subsonic boundary layer of the internal flow, and will probably suppress and smooth a large

pressure drop inside the nozzle, reducing the boundary layer thickness. Therefore, it can be expected that this multi-jet effect will reduce the boundary layer thickness and namely improve nozzle efficiencies. The reduction of each nozzle-separation will result in the nozzle exhaust flow to be equivalent to that of a single nozzle which has the identical total-exit-height. Although the total-exit-height is identical, the multi-nozzle array has the advantage in that its nozzle length can still be kept small, or thin, compared to the single nozzle, in which its length has to be at least twice as large as its height. This point can be one of the most significant advantages of the multi-nozzle array.

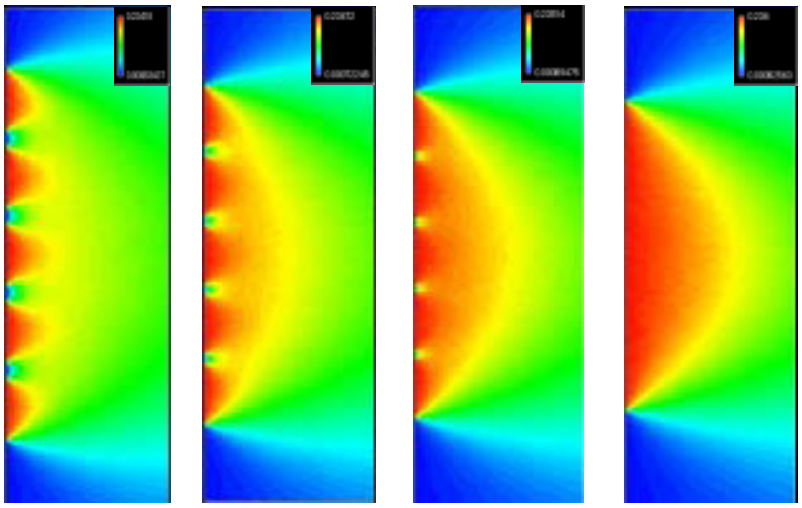

(a) (b) (c) (d)

Figure 3. Typical results of pressure distributions for two-dimensional quintuple nozzle cases for different nozzle-separations, (a) 100 μm, (b) 50 μm, (c) 25 μm, and (d) 0μm

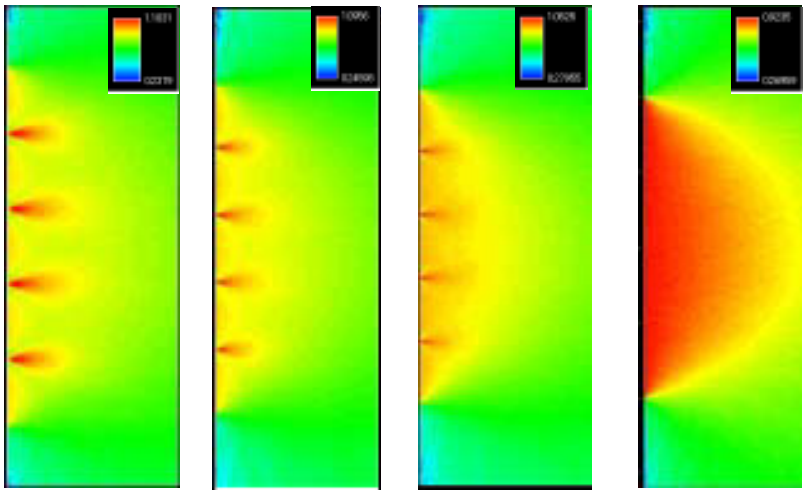

(a) (b) (c) (d)

Figure 4. Typical results of temperature distributions for two-dimensional quintuple nozzle cases for different nozzle-separations, (a) 100 μm, (b) 50 μm, (c) 25 μm, and (d) 0μm

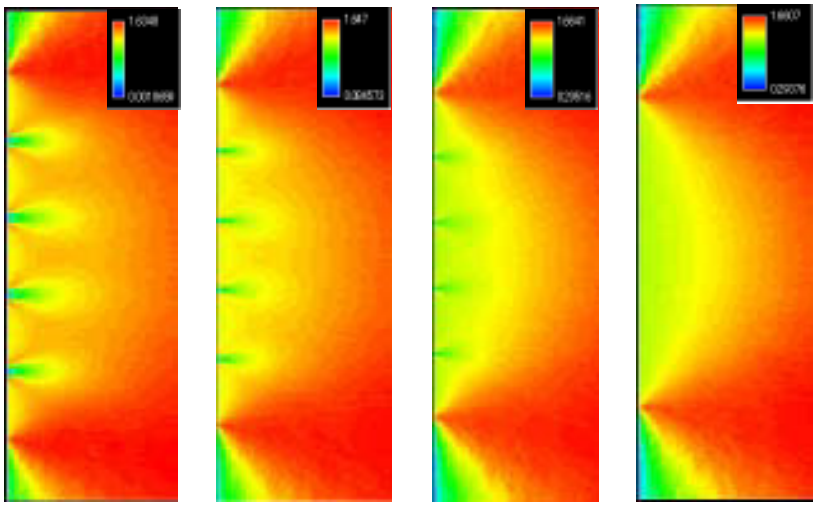

(a) (b) (c) (d)

Figure 5. Typical results of Mach number distributions for two-dimensional quintuple nozzle cases for different nozzle-separations, (a) 100 μm, (b) 50 μm, (c) 25 μm, and (d) 0μm

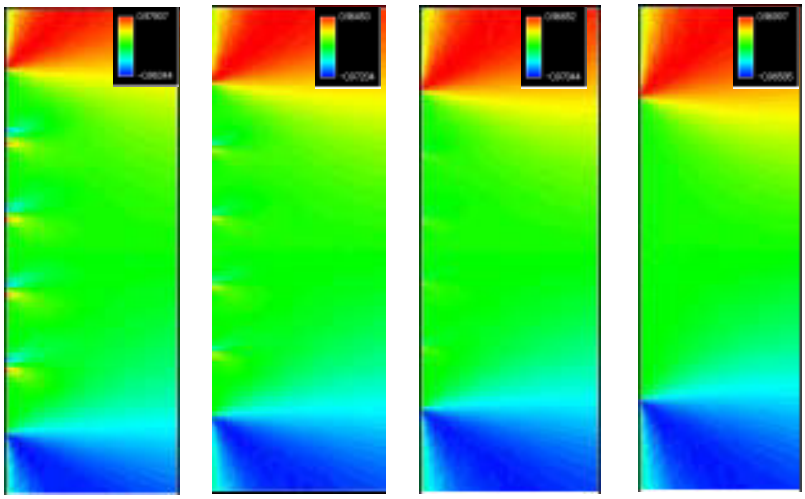

(a) (b) (c) (d)

Figure 6. Normal component distributions of velocity vectors for each nozzle-separation for cases of Figs.3 (a)~(d)

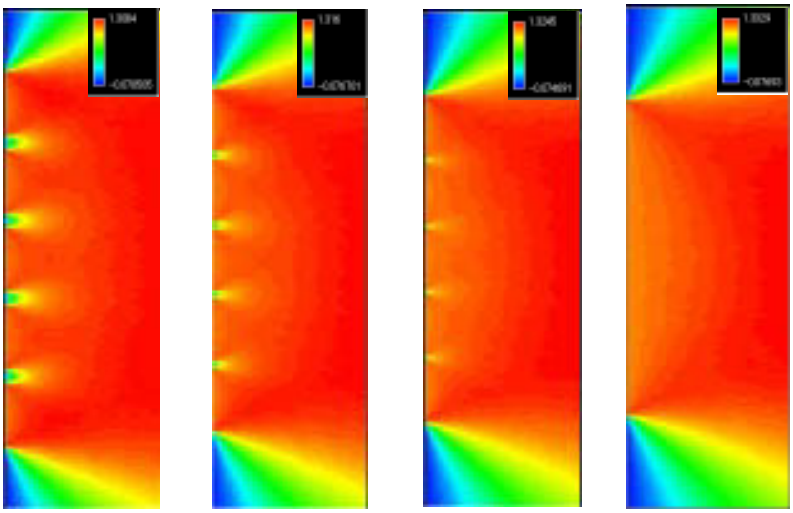

(a) (b) (c) (d)

Figure 7. Axial component distributions of velocity vectors for each nozzle-separation for cases of Figs.3 (a)~(d)

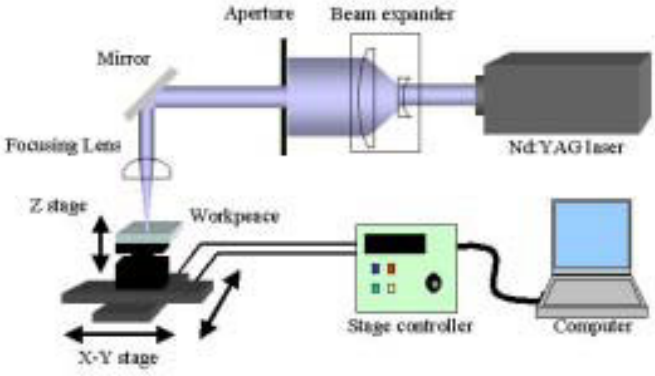

Figure 8. Schematics of UV laser micromachining system for arcjet-nozzles.

III. Micro-Arcjet Machining

A. Microfabrication of Micro-Nozzles with UV Laser beams

For micromachining of micro-nozzles, a laser micromachining system shown in Fig.8 was developed and utilized. In order to minimize and localize thermal influences such as melting and crack formation, and to achieve accurate geometries, a short-pulse ultra-violet laser system was utilized. For the UV laser oscillator, a fifth harmonic generation wave of an Nd:YAG laser beam (Fifth-HG, wavelength 213 nm, NEWWAVE RESEARCH, Tempest–10, repetition rate 10 Hz) was utilized. A specification of the laser system is listed in Table 1. In this system, a

combination of nonlinear optical crystals of KTP ($KTiOPO_4$, potassium titanyl phosphate) (for second harmonic generation, SHG), BBO (β-BaBO4,) (for third harmonic generation, THG) and BBO (for fifth harmonic generation, Fifth-HG) was used for UV generation. The laser pulses were focused with a quartz focusing lens (f = 40 mm) and irradiated onto a workpiece surface in air under an atmospheric pressure as shown in Fig.4. For micromachining of nozzles, a PC controlled X-Y stage was utilized to scan focused laser beams, on which a workpiece was attached. With changing feed speed and number of pulse shots which were programmed in the PC, a designed nozzle configuration could be formed. This procedure giving relative scans between the laser beam and the workpiece surface enabled to micromachine any three dimensional nozzle structures. The minimum feed speed of the stage was 0.2 μm/sec and the maximum scanning length was 100 mm in each axis. A scanning electron microscope (SEM, JOEL JSM5410LV) and a laser microscope (KEYENCE, VK-8500) were used for detailed surface observations and measurements.

Before micromachining the micro-nozzles with laser beams, laser-machining characteristics of hole-drilling, grooving, and surface machining were investigated. In this investigation, geometrical accuracy and thermal influences such as degrees of molten layer thickness and crack formation, not preferred for higher accuracy and quality of surfaces, were evaluated.[19]

Table 1. Specifications of NEWWAVE RESEARCH Nd:YAG Laser: Tempest-10.

Wavelength [nm]		Maximum energy [mJ/pulse]	Pulse width [nsec]
Fundamental	1064	200	3 ~ 5
Second-HG	532	100	
Third-HG	355	50	
Fourth-HG	266	30	
Fifth-HG	213	7	

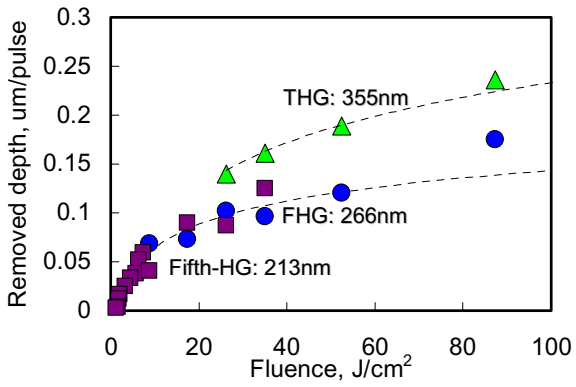

Figure 9. Laser fluence vs removed depth for various lasers.

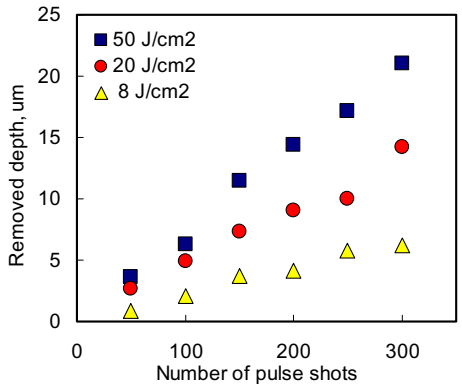

Figure 10. Number of pulse shots vs depth.

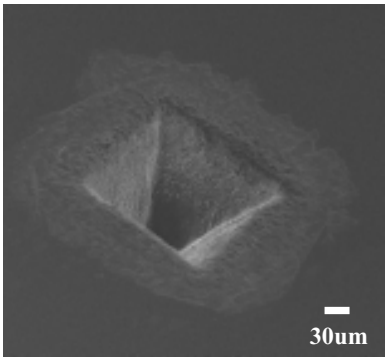

Figure 11. SEM image of a micro-nozzle.

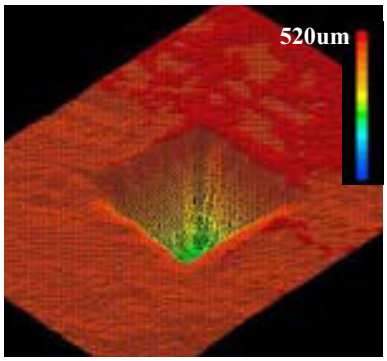

Figure 12. Laser-microscope image of a micro-nozzle.

Relationships between laser fluence and removed depth per pulse for various harmonic waves of Nd:YAG laser beams are shown in Fig.9. These plots were calculated from the removed depth measured by a laser-microscope divided by number of pulse shots for various fluence and wavelength cases of irradiated laser pulses. These plots show the surface removing characteristics of various wavelength lasers at near-threshold fluences below which no ablation on a focal point of the surface can be observed. Above these fluences, i.e., higher than 60 ~ 100 J/cm^2, significant thermal damages such as lots of cracks and melting were observed in each wavelength case.

From the figure it can be seen that there exists a minimum fluence value and a minimum depth for each wavelength case and that these values decrease with reducing the laser wavelength. Little redeposition of molten material around the craters were seen and the cleaner removal of the surface seemed to be possible with the Fifth-HG beam. Therefore, with the Fifth-HG pulses, not only reduction of thermal influences of a laser beam but also laser processing to be controlled in axial direction of the beam was possible, which used to be of essential difficulty with the conventional laser processing. From the results, it was shown that shorter wavelength lasers could remove the surface with lower fluence beams in lower ablation rates. Since a thermal input per pulse from the incident beam to the irradiating spot can be reduced at the low fluence cases, thermal influences, which are not preferred, around the spot can also be reduced. From these results, it is suggested that shorter wavelength lasers are capable for accurate control of the removing depth and also for reduction and limitation of thermal influences. It has been reported that the changes of the removed depth per pulse

Effects of number of pulse shots on removed depth for various laser fluences of Fifth-HG cases estimated with a laser microscope are shown in Fig.10. From the figure, it is shown that the removed depth increases linearly with the pulse shots. Also smaller increments of the removed depth, or accurate etching rates of the surface, can be obtained with changes of pulse shot in lower fluence cases. It is therefore confirmed again that higher accuracy of the depth can be achieved with lower fluence lasers. From these results, it was shown that with controlling the fluence and pulse shots (or scan numbers), the depth, or the removing rate, can be controlled in the axial direction of the laser beam. Depending on optical configurations, the minimum hole diameter obtained by this system was about 7 μm, and typical surface roughness of the removed surface was about 200 nm. With this laser-micromachining system, various sizes of the rectangular nozzles of both quartz and sapphire workpieces were machined.

Figures 11 and 12 show a SEM image and a laser-microscope image of a sapphire micro-nozzle exit, respectively. Sizes of the nozzle are 240 μm in width for the nozzle exit and 520 μm in depth to its throat. In this case, average laser pulse fluence was 5 J/cm^2 for a beam spot of 40 μm in diameter on the workpeace surface. A focal point was set 10 μm below the surface. Feed speed of the X-Y stage was set 100 μm/sec in this case. It can be seen that no cracks and sharp edges were formed on inner- and outer-areas of the nozzle.

B. Structural Advantages of Micro-Arcjet

Figure 13 shows a schematic illustration of a rectangular micro-arcjet nozzle machined in a 1.2 mm thick quartz plate. Sizes of the nozzle are 440 μm in heights of the nozzle exit and constrictor heights of 100 μm. Cross-sectional

schematics of the micro-arcjet nozzles with film electrodes are shown in Fig.14(a). For each anode, a thin film of Au (~ 100 nm thick) was coated by DC discharge PVD in vacuum on a divergent part of the nozzle, as shown in Fig.14(b). As for a cathode, an Au film was also coated on inner wall surface. In this case, a constrictor part of the nozzle was electrically insulated to maintain high voltage mode discharges, as described in the previous section. In all the tests, nitrogen gas was used as the propellant gas.

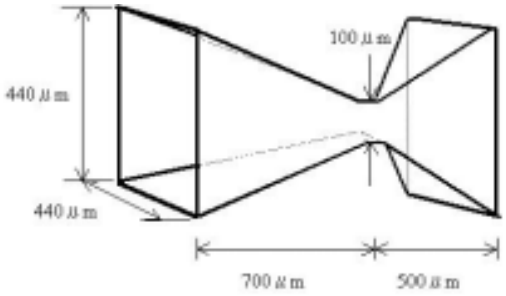

Figure 13. Schematic of a micro-arcjet nozzle.

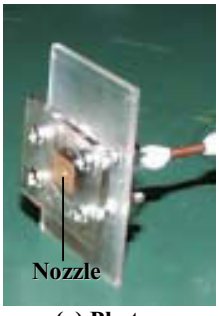

(a) Photo

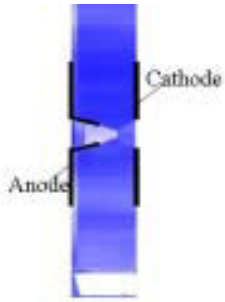

(b) Schematic of nozzle and planar electrodes

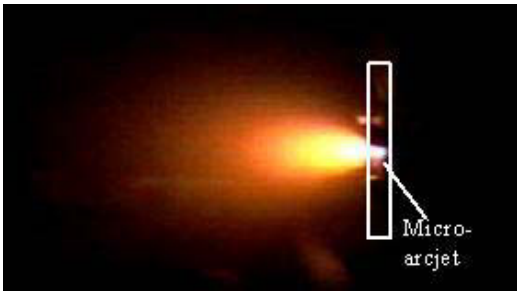

(c) Photo in stable operation

Figure 14. Photos and schematic of micro-arcjet.

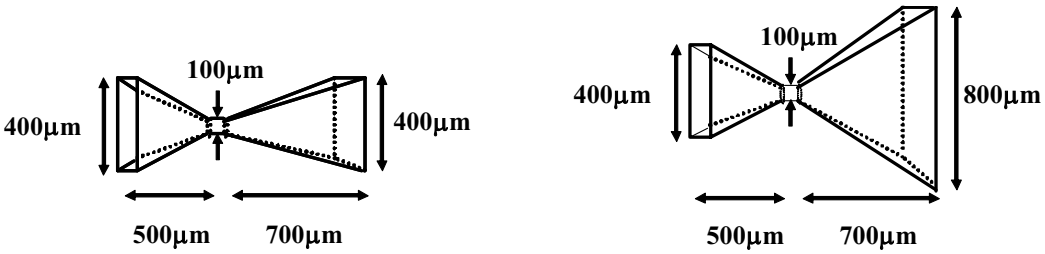

(a) 400 μm-nozzle **(b) 800 μm-nozzle**

Figure 15. Schematic configurations of micro-nozzles with different exit heights examined in thrust performance tests.

In general, a high-melting point metal has been used for a cathode of the arcjet, in which a stable discharge is established with an increased rate of thermal emission of electrons from the heated electrode. On the other hand, under very low-power discharge conditions like this study, it was possible to maintain a stable discharge within a glow discharge mode shown in Fig.14(c), rather than the arc discharge mode, in which it was difficult to maintain a stable discharge for a long time without any thermal damages of an insulator and a nozzle throat, as described in the previous section. Although not shown, the discharge with a conical cathode tended to transit into the arc discharge and namely became unstable. From these findings, it was confirmed that a planar cathode could work better in the operational conditions of this study. In addition, this planar cathode had a structural advantage since it could be simple. Moreover, since the discharge mode was not the arc discharge, no local heating of the electrodes could be observed. No remarkable thermal damages on electrodes and insulators could be seen after the discharge operation. Therefore, no special heat resisting materials was needed for the electrodes and insulators.

IV. Preliminary Operational Test of Micro-Arcjet

As a preliminary investigation, thrust performances of two types of micro-nozzles were tested. Schematic configurations of the micro-nozzles were shown in Fig.15. As shown in these figures, micro-nozzles with different area ratios, or different exit heights of (a) 400 μm and (b) 800 μm, with same constrictor heights of 100 μm, were machined and examined. A thrust performance test was conducted in a vacuum vessel. A calibrated cantilever-type thrust stand consisting of quartz plates was used for the measurement. The specific impulse and the thrust efficiency were calculated using the values of total thrust, thrust of cold gas jet, mass flow rate, and electrical input power.

A. Cold-Gas Thrust Performance Test

Plots of cold-gas thrust (with 0 W input power) and specific impulse versus mass flow rate for both micro-thrusters are shown in Figs.16 (a) and (b), respectively. The cold-gas thrust in both cases increase with propellant mass flow rate up to 0.42 mN for 400μm-nozzle and 0.67 mN for 800μm-nozzle, respectively, for propellant (N_2) mass flow rate of up to 2 mg/sec. The specific impulse varies from 10 to 20 sec for 400μm-nozzle and 10 to 33 sec for 800μm-nozzle, respectively, with propellant mass flow rate. From these results, it was shown that thrust performance of the 800μm-nozzle was higher than those of 400μm-nozzle.

B. Discharging Thrust Performance Test

Since higher thrust performances were obtained with the 800μm-nozzle in the cold-gas tests, a discharging operational test was also conducted for this nozzle configuration. A photo of a discharging plasma plume exhausted from a micro-arcjet nozzle taken by a color CCD camera (30 frames/sec, 30 msec/frame) is shown in Fig.14(c), for mass flow of 0.4 mg/sec, discharge current of 20 mA, discharge voltage of 430 V (input power of 8.6 W, or specific power of 8.6 MW/kg), and plenum pressure of discharging chamber of 50 kPa. As shown in Fig.14, a stable discharge could be achieved. From results of discharge current-voltage characteristics, it was confirmed that the

discharge voltage was almost constant with variation of the current, and the discharge mode was more like that of glow discharge rather than of arc discharge.

Relations of mass flow rate versus thrust and specific impulse for the 800μm-nozzle are shown in Figs.17 (a) and (b), respectively. It was shown that the thrust of both cases rises with mass flow and can be significantly increased with additional input power. On the other hand, the specific impulse of the discharging case decreased with the mass flow, and tended to approach a constant value of the cold-gas case at relatively high mass flow. Since the specific power, or input power of unit mass flow, decreases with the increase of mass flow and total temperature, or enthalpy, of the gas flow must be decreased, the specific impulse decreases. At mass flow of 0.4 mg/sec, a specific impulse was 147 sec giving a thrust efficiency of 7 %.

Although not shown, in various configuration cases, it was confirmed that thrust performance could be significantly influenced, or improved, with the increase of background pressure of the vacuum chamber. For example, the increase of the background pressure of an order of magnitude resulted in improvement of the thrust and specific impulse of 30 % higher, in a typical case. Since the vacuum condition in space cannot be controlled and further extension of a divergent section of the micro-nozzle cannot be tolerated and preferred, nozzle geometry problems of such the under-expanded nozzle are still posing challenging issues to be overcome.

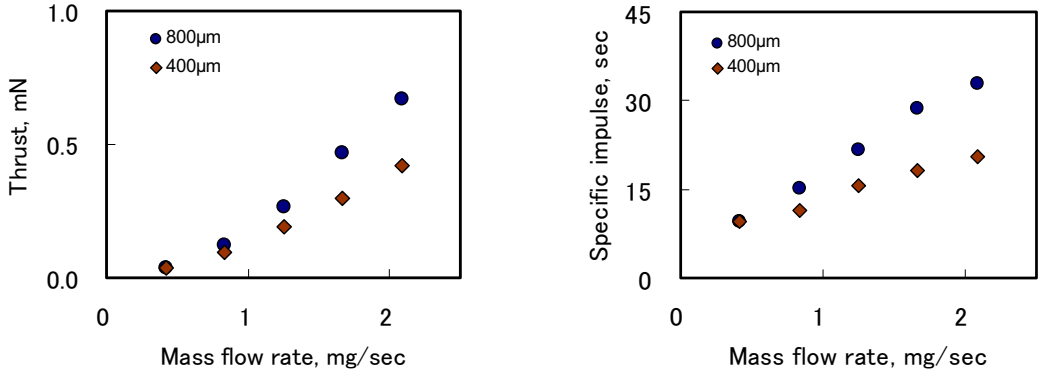

(a) Cold-gas thrust vs mass flow. **(b) Cold-gas specific impulse vs mass flow.**

Figure 16. Plots of cold-gas thrust (with 0 W input power) and specific impulse versus mass flow rate for both micro-thrusters of exit height of 400μm and 800μm.

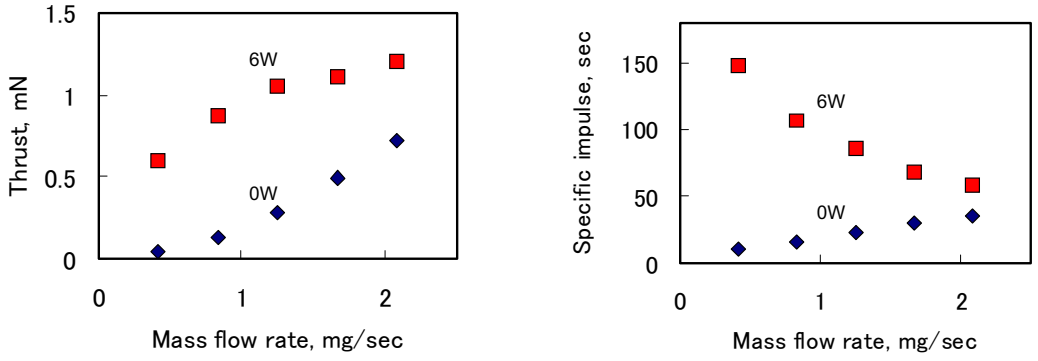

(a) Thrust vs mass flow. **(b) Specific impulse vs mass flow.**

Figure 17. Relations of mass flow rate versus thrust and specific impulse for 800μm-nozzle.

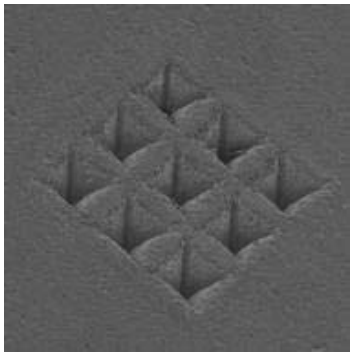

Figure 18. SEM image of a 3 x 3 micro-arcjet array, in which exit height of each nozzle element is 400μm and separations between nozzle edges are 100 μm.

C. Laser Micromachining of Micro-Arcjet Array

Trials of micromachining of a micro-arcjet array with multi-nozzles were conducted. A SEM image of a 3 x 3 micro-arcjet array is shown in Fig.18, in which exit height of each nozzle element is 400 μm and separations between nozzle edges are 100 μm. As shown in this figure, it can be seen that clear and sharp nozzle edges are formed and no remarkable thermal damages such as melting and cracks are observed. The next step of this study is to micromachine more complex nozzle arrays using the present UV laser machining technique and to conduct thrust performance tests of the nozzles.

V. Conclusions

Preliminary DSMC simulations on internal and exhaust nozzle-flow characteristics of micro-arcjet nozzles including multi-mozzle arrays were conducted. It was shown that the use of the multi-nozzle array was effective in suppressing expansion of each under-expanding jet, and in inducing axially confined jets, through the interactions of the jet boundaries, or multi-jet effects. Microfabrication of micro-arcjet nozzles with fifth-harmonic Nd:YAG pulses (wavelength 213 nm) and their operational tests were also conducted. Micro-arcjet nozzles were machined in a 1.2 mm thick quartz plate. Sizes of the nozzle exit were 0.44 mm in height and constrictor height of 0.1 mm. For an anode, a thin film of Au (~ 100 nm thick) was coated by DC discharge PVD in vacuum on divergent part of the nozzle. As for a cathode, an Au film was also coated on inner wall surface. In operational tests, a stable discharge was observed for mass flow of 0.4 mg/sec, input power of 6 W. In this case, plenum pressure of the discharge chamber was 50 kPa. With 6 W input power, thrust obtained was 1.2 mN giving specific impulse of 147 sec with thrust efficiency of 7 %.

References

[1] Micci, M.M., and Ketsdever, A.D. (ed.), Micropropulsion for Small Spacecraft, Progress in Astronautics and Aeronautics Vol.187, American Institute of Aeronautics and Astronautics, 2000.

[2] Myers, R.M., Oleson, S.R., Curren, F.M., and Schneider, S.J., "Small Satellite Propulsion Options," AIAA Paper 94-2997, 1994.

[3] Mueller, J., "Thruster Options for Microspacecraft: A Review and Evaluation of Existing Hardware and Emerging Technologies," AIAA Paper 97-3058, 1997.

[4] Leifer, S., " Overview of NASA's Advanced Propulsion Concepts Activities," AIAA Paper 98-3183, 1998.

[5] Jahn, R.G., Physics of Electric Propulsion, McGraw-Hill, 1968.

[6] Birkan, M.A., "Arcjets and Arc Heaters: An Overview of Research Status and Needs", Journal of Propulsion and Power, Vol.12, No.6, 1996, pp.1011-1017.
[7] Martinez-Sanchez, M., and Pollard, J.E., "Spacecraft Electric Propulsion-An Overview", Journal of Propulsion and Power, Vol.14, No.5, 1998, pp.688-699.
[8] Horisawa, H., and Kimura, I., "Optimization of Arc Constrictor Sizes in Low Power Arcjet Thrusters," AIAA Paper 97-3202, 1997.
[9] Horisawa, H., and Kimura, I., "Influence of Constrictor Size on Thrust Performance of a Very Low Power Arcjet," AIAA Paper 98-3633, 1998.
[10] Horisawa, H., and Kimura, I., "Characterization of a Very Low Power Arcjet," AIAA Paper 99-2435, 1999.
[11] Horisawa, H., and Kimura, I., "Performance Improvement of Very Low Power Arcjets," Proc. 26th IEPC, 1999, pp.345-352.
[12] Horisawa, H., and Kimura, I., "Studies of Very Low Power Arcjets," Chap.6 in Micropropulsion for Small, Progress in Astronautics and Aeronautics Vol.187, American Institute of Aeronautics and Astronautics, 2000, pp.185-197.
[13] Horisawa, H., and Kimura, I., "Very Low Power Arcjet Testing," Vacuum, Vol.59, pp.106-117, 2000.
[14] Horisawa, H. and Kimura, I., "Very Low-Power DC Plasma Jet Microthrusters," AIAA Paper 2001-3791, 2001.
[15] Horisawa, H., and Ashiya, H., and Kimura, I., "Discharge Characteristics of a Very Low-Power Arcjet," IEPC 03-0078, Proceedings of the 28th International Electric Propulsion Conference, 2003.
[16] Ashiya, H., Noda, T., Horisawa, H. and Kimura, I., "Thrust Performances of a Very Low-Power Micro-Arcjet," Proc. Asian Joint Conf. on Propulsion and Power 2004, 2004, pp.358 – 363.
[17] Ketsdever, A. D., "System Consideration and Design Options for Microspacecraft Propulsion System," Chap.4 in Micropropulsion for Small, Progress in Astronautics and Aeronautics Vol.187, American Institute of Aeronautics and Astronautics, 2000, pp.139-163.
[18] Horisawa, H., Emura, H., and Yasunaga, N., "Surface machining characteristics of sapphire with fifth harmonic YAG laser pulses," Vacuum, Vol.73, 2004, pp.661-666.